Color monogenic wavelet representation based on a tensor-like use of the riesz transform: application to image coding

Raphaël Soulard, Philippe Carré

Color monogenic wavelet representation based on a tensor-like use of the Riesz transform : application to image coding

Raphaël Soulard and Philippe Carré

Abstract We propose a new extension of monogenic analysis to multi-valued signals like color images. This generalization is based on an analogy between the Riesz transform and structure tensors and takes advantage of the well defined vector differential geometry. Our color wavelet transform is non-marginal and its coefficients - separated into amplitude, phase, orientation and local color axis - have interesting physical interpretation in terms of local energy, contour model, and colorimetric features. An image coding application is proposed as a practical study.

1 Introduction

Color images are most often handled by working either on intensity or with *marginal* schemes (Marginal schemes consist in applying the same process independently on each color channel [1]). Those methods are sometimes unable to consider some contours, and may also introduce false colors. Yet color information is fundamental in some applications such as medical imaging for instance [14, 4].

Differential approaches are more flexible and allow analyzing vector functions of any dimension within the Riemannian manifolds framework [15]. The vector structure tensor leads to efficient contour detection and adaptive smoothing [18] by handling color pixels as entities.

Definitions about 2D signals showed that the 2D *phase* and *frequency* concepts can lead to interesting local geometric analysis of grayscale images tied to a physical interpretation [7, 2, 5]. Monogenic wavelets [20] perform multiscale local phase analysis. Unfortunately no color definition exists so far.

We propose to get the best of both worlds by injecting the color structure tensor formalism into monogenic wavelets. This paper provides a non-trivial color exten-

XLIM-SIC Dept., Bat. SP2MI, Téléport 2, Bvd Marie et Pierre Curie, BP 30179, 86962 Chasseneuil CEDEX, France e-mail: raphael.soulard@univ-poitiers.fr

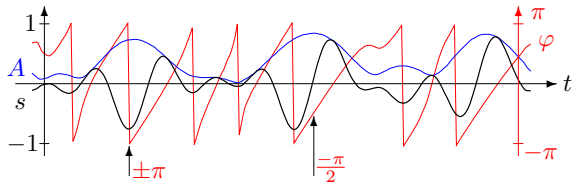

Fig. 1 Analytic signal $A(t)e^{\varphi(t)t}$ associated to a scalar signal $s(t)$. An 'inverted pulse' is coded by $\varphi = \pm\pi$ at the amplitude's maximum (first arrow); an increasing slope is coded by $\varphi = -\frac{\pi}{2}$ (second arrow).

sion of monogenic signal and wavelets to perform coherent multiscale color 2D phase analysis. This definition is an improvement of our previous work [17].

Special Notations:
- Complex numbers : $z = a + \mathbf{j}b = |z|e^{\mathbf{j}\arg\{z\}}$
- 2D coordinate in bold : $\mathbf{x} = [x_1 \;\; x_2] \quad \omega = [\omega_1 \;\; \omega_2]$
- Classical Fourier transform : $s \overset{\mathscr{F}}{\longleftrightarrow} \hat{s} = \mathrm{TF}\{s\}$

2 Multiresolution monogenic analysis

This section recalls the classical *analytic/monogenic signal* concepts and the monogenic wavelets proposed in [20]. Further details will be found in [6, 7, 5, 20].

2.1 Analytic and monogenic signal

The analytic signal $s_A(t)$ associated to a real signal $s(t)$ reads:

$$s_A(x) = s(x) + \mathbf{j}\{\mathscr{H}s\}(x) = A(x)e^{\mathbf{j}\varphi(x)} \tag{1}$$

$$\text{with the Hilbert transform :} \quad \{\mathscr{H}s\}(x) \overset{\mathscr{F}}{\longleftrightarrow} -\mathbf{j}\,\mathrm{sign}(\omega)\hat{s}(\omega) \tag{2}$$

The analytic signal is an amplitude/frequency modulation model mostly used in communications. But another interpretation in terms of *local structure* is possible [7, 2]. As illustrated Fig. 1, amplitude A conveys the relative presence of local energy while instant phase φ encodes some shape information. More precisely, $\varphi = 0$ or $\pm\pi$ indicates 'pulse'-like pieces of signal whereas $\varphi = \pm\frac{\pi}{2}$ indicates 'slopes'. This geometric interpretation motivated researchers to define a 2D extension to perform AM/FM image analysis. The most successful one is the monogenic signal.

The Riesz transform of a 2D signal s is made of two parts s_{R_1} and s_{R_2}:

$$\{\mathscr{R}s\}(\mathbf{x}) = s_R(\mathbf{x}) = s_{R_1} + \mathbf{j}s_{R_2} \overset{\mathscr{F}}{\longleftrightarrow} (\omega_2 - \mathbf{j}\omega_1)\|\omega\|^{-1}\hat{s}(\omega) \tag{3}$$

Note that this is the $\mathbb{C}$ embedding of the Riesz transform according to [11][1]. The monogenic signal s_M associated to s reads:

$$s_M = [s \;\; s_{R_1} \;\; s_{R_2}] = A[\cos\varphi \;\; \sin\varphi\cos\theta \;\; \sin\varphi\sin\theta] \tag{4}$$

where $\theta = \arg\{s_R\} \in [-\pi;\pi[$ is the local Riesz orientation along which a 1D Hilbert analysis is intrinsically done. This 1D analysis can be written:

$$s_A(\mathbf{x}) = s(\mathbf{x}) + \mathbf{j}|s_R(\mathbf{x})| = A(\mathbf{x})e^{\mathbf{j}\varphi(\mathbf{x})} \tag{5}$$

Amplitude of the monogenic signal conveys local presence of some geometrical elements. The θ-phase gives the corresponding local orientation (we will see that it is equal to a gradient direction). The φ-phase results from an intrinsic Hilbert analysis along orientation θ. So the signal model here is an A-strong structure that is oriented along θ and looking like rather an *edge* ($\varphi \approx \pm\pi/2$) or a *line* ($\varphi \approx 0$ or π). Note that phase based line/edge analysis was discussed in [7, 10].

Monogenic representation is well suited to analyze *narrow-band* signals, so it is natural to use it jointly with *subband* decomposition in order to handle any image.

2.2 Monogenic wavelet transform (MWT)

The scheme of [20] performs multiresolution monogenic analysis by using two parallel filterbanks. One 'primary' transform and a so-called 'Riesz-Laplace' wavelet transform. Multiresolution analyses are built around the nearly isotropic polyharmonic B-spline of [22]:

$$\beta_\gamma \overset{\mathscr{F}}{\longleftrightarrow} \left[4(\sin^2\frac{\omega_1}{2} + \sin^2\frac{\omega_2}{2}) - \frac{8}{3}\sin^2\frac{\omega_1}{2}\sin^2\frac{\omega_2}{2}\right]^{\frac{\gamma}{2}} \|\omega\|^{-\gamma} \tag{6}$$

which is a valid scaling function. The wavelet for the primary decomposition ψ is a Mexican hat-like nearly isotropic function and the 'Riesz-Laplace' wavelet ψ' is derived from it:

$$\psi(\mathbf{x}) = (-\Delta)^{\frac{\gamma}{2}}\,\beta_{2\gamma}(2\mathbf{x}) \qquad \psi' \overset{\mathscr{F}}{\longleftrightarrow} \frac{\mathbf{j}\omega_1 + \omega_2}{\|\omega\|}\hat{\psi}(\omega) \tag{7}$$

where the fractional Laplacian operator is defined by:

$$(-\Delta)^\alpha s \overset{\mathscr{F}}{\longleftrightarrow} \|\omega\|^{2\alpha}\hat{s} \tag{8}$$

Let $\psi_{i,\mathbf{k}}(\mathbf{x}) = 2^i\psi(2^i\mathbf{x} - \mathbf{k}/2)$ be the scaled and shifted version of ψ (same for ψ'). It is shown [20] that $\psi_{i,\mathbf{k}}$ and $\psi'_{i,\mathbf{k}}$ form two wavelet frames ensuring perfect reconstruction and orthogonality across scales. Their *operator-like behavior* induces:

[1] This choice will help to define proper Riesz-based complex wavelets.

$$\langle s, \psi_{i,\mathbf{k}} \rangle = (\psi_i * s)(2^{-(i+1)}\mathbf{k}) \tag{9}$$

$$\langle s, \psi'_{i,\mathbf{k}} \rangle = \mathscr{R}(\psi_i * s)(2^{-(i+1)}\mathbf{k}) \tag{10}$$

This means that wavelet coefficients form an exact monogenic signal at each scale. Both decompositions are merged into 3-vectors and turned into polar coordinate according to eq. (4) as illustrated Fig. 2. Interpretation of coefficients is the same

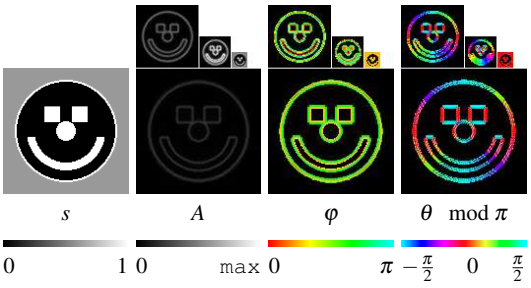

Fig. 2 MWT of image s. Orientation θ is shown modulo π for visual convenience. Phase values of small coefficients have no sense and are numerically unstable so they are replaced by black pixels.

as explained for the monogenic signal but now concerns different scales of the image. The 'pyramid' design of this wavelet transform helps to achieve near rotation invariance by the use of a unique 2D wavelet for each transform [21]. It is remarkable that this approximation does not produces serious artifacts in the representation of 'round' objects like those of figure 2. Dyadic downsampling is done at the low frequency branch leading to a total redundancy of 4:1.

This representation clearly fails to handle color images. Applying it on intensity of an image would induce a serious loss of information around isoluminant contours. Using it marginally would have no more sense by making independent geometric analyses on each color channel. In this case some processing such as thresholding would introduce false colors. We propose an extension that keeps the 1D phase interpretation and yields a coherent color orientation.

3 Extending to color images

This section aims at defining a color counterpart of the monogenic framework. Based on a link with the gradient and structure tensor features, we extract Riesz norm and direction from the well known color structure tensor formalism [3, 13]. This concept has been successfully applied in various color applications such as inpainting and regularization [18]. The second step is to define the corresponding Hilbert analysis that completes the model.

3.1 Color Riesz features

First let us recall definitions of the gradient

$$\nabla s = \begin{bmatrix} \frac{\partial s}{\partial x} & \frac{\partial s}{\partial y} \end{bmatrix} = [s_x \;\; s_y] \overset{\mathscr{F}}{\longleftrightarrow} [\mathbf{j}\omega_1 \hat{s} \;\; \mathbf{j}\omega_2 \hat{s}] \tag{11}$$

and its associated structure tensor $T = h * [\nabla s]^T [\nabla s]$

$$T(s) = \begin{bmatrix} h * s_x^2 & h * s_x s_y \\ h * s_x s_y & h * s_y^2 \end{bmatrix} = \begin{bmatrix} T_{11} & T_{12} \\ T_{12} & T_{22} \end{bmatrix} \tag{12}$$

tied to the smoothing kernel h. Eigenvalues and eigenvectors of T give information about direction and amplitude of the local maximum variation:

- Eigenvalues $\lambda_\pm = \left(T_{11}+T_{22} \pm \sqrt{(T_{22}-T_{11})^2+4T_{12}^2}\right)/2$;
- Gradient norm and direction $\mathscr{N} = \sqrt{\lambda_+ + \lambda_-}$ $\qquad \theta_+ = \frac{1}{2}\arg\{T_{11}-T_{22}+\mathbf{j}2T_{12}\}$;

Now let us build the tensor $T_R = [s_{R_1} \;\; s_{R_2}]^T [s_{R_1} \;\; s_{R_2}]$ formed with the Riesz components of s. Construction from Unser *et. al.* [20] and the work in [9] reveal a link between Riesz and gradient. Equations (3), (8) and (11) give:

$$\mathscr{R}s = \left(-(-\Delta)^{-\frac{1}{2}} s_x\right) + \mathbf{j}\left(-(-\Delta)^{-\frac{1}{2}} s_y\right) \tag{13}$$

The involved smoothing operation is the linear operator $-(-\Delta)^{-\frac{1}{2}}$ whose Fourier response is $1/\|\omega\|$ (see eq. (8)). This means that the Riesz transform is equivalent to a smoothed gradient *or* the gradient of a smoothed version of s, so our Riesz-based tensor reads the following relation:

$$T_R(s) = T(-(-\Delta)^{-\frac{1}{2}} s) \tag{14}$$

Since the smoothing is isotropic, the orientation estimation is equivalent in both the gradient case and the Riesz case. As a consequence, we can say that the Riesz norm and direction are equivalent to gradient features. This suggests the use of the color structure tensor formalism to retrieve meaningful Riesz features from a color image.

The color structure tensor is the central tool of color differential approaches [3, 13, 15, 18]. Given a color image $\mathbf{s} = (s^r, s^g, s^b)$, consider its marginal gradients along x and y $(s_x^r, s_x^g, s_x^b, s_y^r, s_y^g, s_y^b)$. The color structure tensor is defined as follows:

$$T = \begin{bmatrix} a & b \\ b & c \end{bmatrix} \quad \text{with} \quad \begin{array}{l} T_{11} = (s_x^r)^2 + (s_x^g)^2 + (s_x^b)^2 \\ T_{12} = s_x^r s_y^r + s_x^g s_y^g + s_x^b s_y^b \\ T_{22} = (s_y^r)^2 + (s_y^g)^2 + (s_y^b)^2 \end{array} \tag{15}$$

Norm and direction of local maximum variation can still be retrieved by the eigen decomposition of T. It is now trivial to derive the Riesz case since the color tensor is the sum of marginal tensors $T = T_r + T_g + T_b$. The Riesz transforms on red, green

and blue channels can obviously be combined to form a smoothed version of T. The color counterpart of the Riesz transform is then $s_R^{\text{color}} = \mathscr{N}\, e^{\mathbf{j}\theta}$ with:

$$\mathscr{N}^2 = \sum_{c\in\{r,g,b\}} (s^c_{R_1})^2 + (s^c_{R_1})^2 \tag{16}$$

$$\theta = \frac{1}{2}\arg\left\{ \left(\sum_{c\in\{r,g,b\}} (s^c_{R_1})^2 - (s^c_{R_2})^2 \right) + \mathbf{j}\left(2\sum_{c\in\{r,g,b\}} s^c_{R_1} s^c_{R_2} \right) \right\} \tag{17}$$

The advantage of this generalization is that the structure tensor gives a coherent oriented analysis of *all* color discontinuities. This particular case of color structure tensor is the link with the monogenic framework. A 1D Hilbert analysis can now be made between s and $|s_R^{\text{color}}| = \mathscr{N}$ so we can adapt it to color images.

3.2 Color monogenic analysis

The key idea is to handle Euclidean norm $\|\mathbf{s}\| = \sqrt{s_r^2+s_g^2+s_b^2}$. In the scalar case, this reduces to $|s|$. It is then interesting to rewrite the scalar model while separating absolute value and sign of s:

$$s = \underbrace{\sqrt{s^2+\mathscr{N}^2}}_{A} \cos\Big(\underbrace{\arg\{s+\mathbf{j}\mathscr{N}\}}_{\varphi\in[0;\pi[} \Big) \tag{18}$$

$$= \underbrace{\sqrt{|s|^2+\mathscr{N}^2}}_{A} \cos\Big(\underbrace{\arg\{|s|+\mathbf{j}\mathscr{N}\}}_{\varphi_2\in[0;\frac{\pi}{2}[} \Big) \underbrace{s/|s|}_{\text{“sign”}} \tag{19}$$

The new phase φ_2 is a restricted version of φ to interval $[0;\frac{\pi}{2}]$. Fortunately we keep interesting qualitative information of edge/line discrimination. The vector counterpart relies on the separation of s into its Euclidean norm and its ‘color axis’ $\vec{u}$:

$$\mathbf{u} = \mathbf{s}/\|\mathbf{s}\| = [\cos\alpha\ ,\ \sin\alpha\cos\beta\ ,\ \sin\alpha\sin\beta] \tag{20}$$

To the best of our knowledge this concept of color axis is new, as a consequence of our tensor-based color extension. The color monogenic model becomes:

$$\mathbf{s} = \sqrt{\|\mathbf{s}\|^2+\mathscr{N}^2}\cos\big(\arg\{\|\mathbf{s}\|+\mathbf{j}\mathscr{N}\}\big)\,\mathbf{u} \tag{21}$$

The main 4 components of the new color monogenic signal are therefore $\mathbf{s}_M^{\text{color}} = [\, s_r\ ,\ s_g\ ,\ s_b\ ,\ \mathscr{N}\,]$, and their spherical coordinates are:

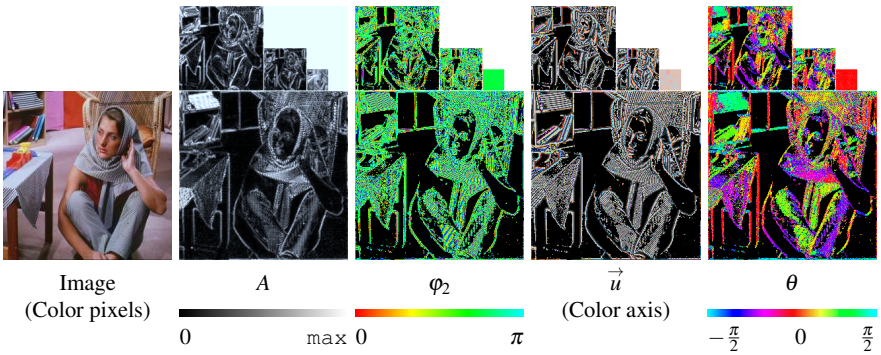

Fig. 3 Color monogenic wavelet transform on `barbara` image.

$$\begin{aligned}
&\text{Amplitude}: A = \sqrt{s_r^2 + s_g^2 + s_b^2 + \mathcal{N}^2} \in [0; +\infty[\\
&\text{1D Phase}: \quad \varphi_2 = \arg\{\|\mathbf{s}\| + \mathbf{j}\mathcal{N}\} \in [0; \tfrac{\pi}{2}[\\
&\text{Color axis}: \begin{cases} \alpha = \arg\{s_r + \mathbf{j}\sqrt{s_g^2 + s_b^2}\} \in [0; \pi[\\ \beta = \arg\{s_g + \mathbf{j}s_b\} \in [-\pi; \pi[\end{cases}
\end{aligned} \tag{22}$$

Color Riesz orientation θ may also be used in practice.

3.3 Color monogenic wavelets

The extension to the wavelet domain is trivial since the above construction relies on a marginal Riesz transform (non marginality occurs when combining marginal outputs into meaningful data). We define the two vector - color - wavelets ψ and ψ' and their associated coefficients for scale i and position $\mathbf{k}$:

$$\psi = [\psi \;\; \psi \;\; \psi] \qquad \psi' = [\psi' \;\; \psi' \;\; \psi'] \tag{23}$$

$$\mathbf{w}_{i,\mathbf{k}} = [r_{i,\mathbf{k}} \;\; g_{i,\mathbf{k}} \;\; b_{i,\mathbf{k}}] \qquad \mathbf{w}'_{i,\mathbf{k}} = [r'_{i,\mathbf{k}} \;\; g'_{i,\mathbf{k}} \;\; b'_{i,\mathbf{k}}] \tag{24}$$

And the monogenic signal is for each scale i:

$$\mathbf{w}_M(\mathbf{k}) = [r_{i,\mathbf{k}} \;\; g_{i,\mathbf{k}} \;\; b_{i,\mathbf{k}} \;\; \|\mathbf{w}'_{i,\mathbf{k}}\|] \tag{25}$$

Then A, φ and $\vec{u}$ can be retrieved with eq. (22) by replacing s_r (resp. s_g, s_b and $\mathcal{N}$) with $r_{i,\mathbf{k}}$ (resp. $g_{i,\mathbf{k}}$, $b_{i,\mathbf{k}}$ and $\|\mathbf{w}'_{i,\mathbf{k}}\|$). Local orientation θ can be obtained from eq. (17) by replacing $s^c_{R_1} + \mathbf{j}s^c_{R_2}$ with $c'_{i,\mathbf{k}}$.

See examples of MWT on Fig. 3. Amplitude's invariance property is linked to a high visual coherence w.r.t. image contours. Discontinuities of isoluminance like the boundary between green and red big disks in first image are well detected thanks to the use of the structure tensor formalism. Phase of small amplitude coefficients

is irrelevant thus not displayed. Value of φ_2 at the position of maximum amplitude reveals the kind of discontinuity as explained section 2.1. This rich description of discontinuities is exclusive to the phase concept [10] and so makes this signal processing approach competitive. In practice φ_2 is hard to visualize because of its fast variation. Discontinuities occur from one color to another - drawing an axis in the color space. This axis is represented by the unit vector $\vec{u}$ that completes the phase data. In most cases $\vec{u}$ is slowly varying. Gradient-based θ is the local color structure main spatial direction.

This monogenic representation of color images is consistent with the grayscale definition in terms of 'signal' interpretation (phase and orientation) while taking advantage of a well defined differential model for handling vector signals. We propose to use this fine representation of visual information in an image coding context.

4 Use for coding purpose

Compression is a great success of wavelets with JPEG-2000 algorithm for example. One of the fundamental steps in such a scheme is the coding method consisting in selecting coefficients and representing them numerically (quantization). Specificity of monogenic data being in polar coordinate makes selection and quantization of color monogenic coefficients far from straightforward. First, literature is quite poor about quantization or even statistical modeling of a Euclidean norm and three angles. Second, the redundancy of monogenic analysis makes it not dedicated *a priori* to compression. In a previous work [16] we proposed an experimental quantization method for *quaternionic* wavelets (grayscale) that gave encouraging results for 'lossy' compression. The phase data turns out to be very light to code without introducing serious visible artifacts. We expect the color monogenic transform to give analogous results for color images.

Experiments

As a first step to the use of our transform for coding, we propose some experimental results with uniform quantization to get an idea of the number of bits needed to properly code wavelet coefficients. This is also a way to better understand the kind of visual content that is coded by the various data. Note that our quantization schemes are not comparable with state-of-the-art compression methods that also include entropy coding and various algorithmic tricks to reduce the amount of data.

We use 4 fixed numbers of bits $(B_A, B_{\varphi_2}, B_\alpha, B_\beta)$ for the whole transform, each one related to a coordinate. Decomposition level is 4 and the low frequency subband is not degraded. We show on figure 4 (first column) that a uniform quantization on 6 bits (resp. 2, 3, 4) for A (resp. φ_2, α and β) induces almost no visible artifact in reconstructed image. This choice corresponds to a quantization step of $\pi/8$ for the phase and color axis angles, which may be thought quite coarse. Total number of

Quantization	circles	mandrill	barbara
$B_A = 6$ $B_{\varphi_2} = 2$ $B_\alpha = 3$ $B_\beta = 4$	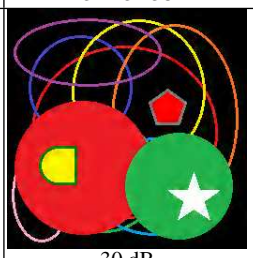	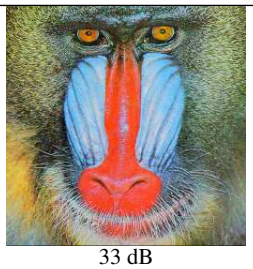	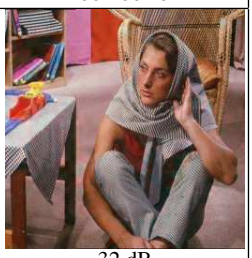
PSNR:	30 dB	33 dB	32 dB
$B_A = 3$ $B_{\varphi_2} = 2$ $B_\alpha = 3$ $B_\beta = 4$	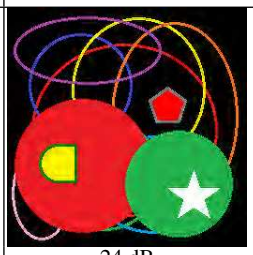	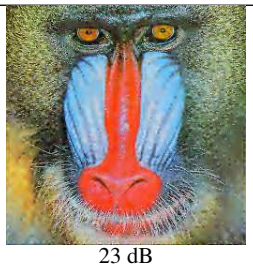	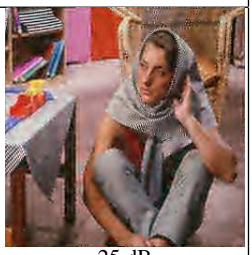
PSNR:	24 dB	23 dB	25 dB
$B_A = 6$ $B_{\varphi_2} = 1$ $B_\alpha = 3$ $B_\beta = 4$	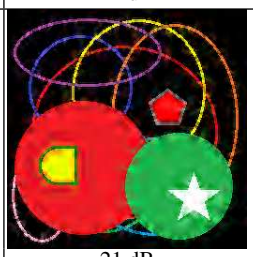	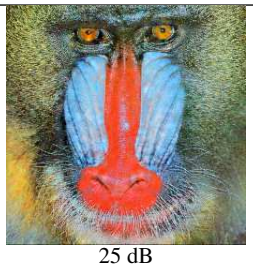	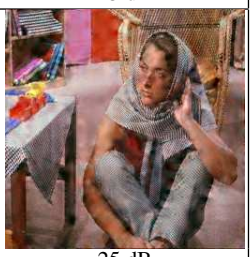
PSNR:	21 dB	25 dB	25 dB
$B_A = 6$ $B_{\varphi_2} = 2$ $B_\alpha = 1$ $B_\beta = 2$	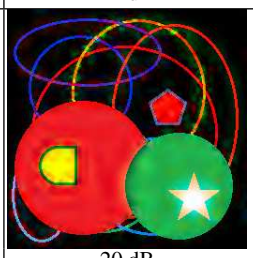	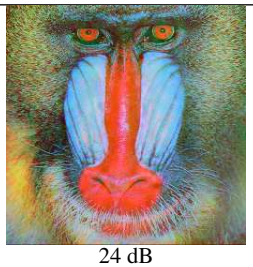	
PSNR:	20 dB	24 dB	23 dB

Fig. 4 Basic uniform quantization of $(A, \varphi_2, \alpha, \beta)$ on $(B_A, B_{\varphi_2}, B_\alpha, B_\beta)$ bits.

bits needed to code the image is then $16/9 \times (6+2+3+4) \approx 27$ times the number of pixels. This amount of data is comparable to the original 24 bit coding of raw color image. We clearly position the work in the 'lossy' case, as usually done with redundant representations.

By degrading amplitude A (second row) we observe the classical pseudo-Gibbs effect introducing oscillations at borders of image `circles`. This also smoothes

textured areas like the lower left corner of `mandrill`. So A is analogous to usual wavelet coefficients, while preserving colors thanks to the non-marginality.

Hard quantization of the phase φ_2 produces visually annoying 'wet paper' effect. Around discontinuities, phase is expected to be coherent across scales [12]. Sometimes the round off due to quantization may increase small differences of phase between scales, resulting in visible local bad alignments of graphical elements. Phase error is more serious in coarsest scales, since they imply phase-shifting on a large neighboring. This explains altered sharp contours and preserved textures. Again, color is strikingly coherent like the green-red border between the big disks of `circles`.

Finally, by quantizing color axis only on $1+2=3$ bits we naturally introduce false colors. This confirms that α and β encode some true colorimetric information being independent from A and φ_2.

This experiment corroborates the aforementioned theoretical interpretation of coefficients, by illustrating the kind of information being carried in each component. It also shows that our transform is stable with quantization and that it can be introduced in a whole coding scheme. We can independently control contours' sharpness and quality of colors with a reasonable number of bits.

5 Conclusion

This paper presents a new proposition of color MWT by extending the grayscale MWT of Unser *et. al.* The definition is strongly linked to color structure tensor while offering a *signal processing* interpretation through the local phase concept. The transform is invariant by translation and rotation and gives coherent multiscale representation of color structures. This non marginal scheme avoids classical problem of false color and also detects all color contours, which is confirmed in an image coding application.

The construction can easily be extended to the general multichannel case by considering general vector structure tensors. It may also be interesting to use truly isotropic decompositions such as those of [8, 19], though they do not yet offer a unique reconstruction. We suggest now to exploit this fine representation in practice. Our prospects include applications in texture analysis and compression. In particular, statistical modeling of phase angles by circular probability laws.

Acknowledgment

This work is part of the French ANR project VERSO-CAIMAN. We thank the French region Poitou-Charentes for participating. We would like to thank the anonymous reviewers for their valuable remarks.

References

1. A. C. Bovik. *Handbook of Image and Video Processing*. Academic Press, May 2000.
2. T. Bülow. Hypercomplex spectral signal representation for the processing and analysis of images. *Thesis*, August 1999.
3. S. Di Zenzo. A note on the gradient of a multi-image. *Computer Vision, Graphics, and Image Processing*, 33(1):116 – 125, 1986.
4. F. Ercal, A. Chawla, W. Stoecker, H.-C. Lee, and R. Moss. Neural network diagnosis of malignant melanoma from color images. *IEEE Trans. Biomed. Eng.*, 41(9):837 –845, sept. 1994.
5. M. Felsberg and G. Sommer. The monogenic signal. *IEEE Trans. Signal Process.*, 49(12):3136–3144, 2001.
6. D. Gabor. Theory of communication. *JIEE*, 93(3):429–459, 1946.
7. G. H. Granlund and H. Knutsson. *Signal processing for computer vision*. Kluwer, 1995.
8. S. Held, M. Storath, P. Massopust, and B. Forster. Steerable wavelet frames based on the riesz transform. *IEEE Trans. Image Process.*, 19(3):653 –667, march 2010.
9. U. Köthe and M. Felsberg. Riesz-transforms versus derivatives: On the relationship between the boundary tensor and the energy tensor. *R. Kimmel, N. Sochen, J. Weickert (Eds.): Scale Space and PDE Methods in Computer Vision, Proc. Scale-Space 2005, Lecture Notes in Computer Science 3459, pp. 179-191, Berlin: Springer*, 2005.
10. P. Kovesi. Edges are not just steps. In *Proc. 5th Asian Conference on Computer Vision (ACCV'02)*, pages pp 822–827, Jan 2002.
11. K. G. Larkin, D. Bone, and M. A. Oldfield. Natural demodulation of two-dimensional fringe patterns: I. general background to the spiral phase quadrature transform. *Journal of the Optical Society of America*, 18 (8):1862–1870, 2001.
12. M. Morrone and D. Burr. Feature detection from local energy. *Pat. Rec. Lett.*, 6:303–313, 1987.
13. G. Sapiro and D. L. Ringach. Anisotropic diffusion of multivalued images with applications to color filtering. *IEEE Trans. Image Process.*, 5(11):1582–1586, 1996.
14. T. Shindenwolf, W. Stolz, R. Albert, W. Abwayr, and H. Harms. Classification of melanocytic lesions with colour and texture analyses using digital image processing. *The international Academy of Cytology; Analytical and Quantitative Cytology and Histology*, 15(1):1–11, 1993.
15. N. Sochen, R. Kimmel, and R. Malladi. A general framework low level vision. *IEEE Trans. Image Process.*, 7:310–318, 1998.
16. R. Soulard and P. Carré. Quaternionic wavelets for image coding. In *Proc. European Sig. Proc. Conf. (EUSIPCO'10)*, pages 125–129, Aalborg, Denmark, 8 2010.
17. R. Soulard and P. Carré. Color monogenic wavelets for image analysis. In *Proc. IEEE Int'l Conf. on Image Processing*, pages 277–280, Brussels, Belgium, September 2011.
18. D. Tschumperlé and R. Deriche. Vector-valued image regularization with pdes: A common framework for different applications. *IEEE Trans. Pattern Anal. Mach. Intell.*, 27(4):506–517, 2005.
19. M. Unser, N. Chenouard, and D. Van De Ville. Steerable pyramids and tight wavelet frames in $l_2(\setminus^d)$. *IEEE Trans. Image Process.*, 20(10):2705–2721, October 2011.
20. M. Unser, D. Sage, and D. Van De Ville. Multiresolution monogenic signal analysis using the riesz-laplace wavelet transform. *IEEE Trans. Image Process.*, 18(11):2402–2418, November 2009.
21. M. Unser and D. Van De Ville. The pairing of a wavelet basis with a mildly redundant analysis via subband regression. *IEEE Trans. Image Process.*, 17(11):1–13, November 2008.
22. D. Van De Ville, T. Blu, and M. Unser. Isotropic polyharmonic b-splines: Scaling functions and wavelets. *IEEE Trans. Image Process.*, 14 :(11):1798–1813, 2005.